Hindawi Publishing Corporation
Mathematical Problems in Engineering
Volume 2016, Article ID 8139273, 11 pages
http://dx.doi.org/10.1155/2016/8139273

Research Article

Fault Diagnosis of Motor Bearing by Analyzing a Video Clip

Siliang Lu,[1,2] Xiaoxian Wang,[3] Fang Liu,[1,2] Qingbo He,[4] Yongbin Liu,[1,2] and Jiwen Zhao[1,2]

[1]*College of Electrical Engineering and Automation, Anhui University, Hefei, Anhui 230601, China*
[2]*National Engineering Laboratory of Energy-Saving Motor & Control Technology, Anhui University, Hefei, Anhui 230601, China*
[3]*The 43rd Research Institute, China Electronics Technology Group Corporation, Hefei, Anhui 230088, China*
[4]*Department of Precision Machinery and Precision Instrumentation, University of Science and Technology of China, Hefei, Anhui 230026, China*

Correspondence should be addressed to Fang Liu; ufun@ahu.edu.cn

Received 6 January 2016; Accepted 9 March 2016

Academic Editor: Anders Eriksson

Conventional bearing fault diagnosis methods require specialized instruments to acquire signals that can reflect the health condition of the bearing. For instance, an accelerometer is used to acquire vibration signals, whereas an encoder is used to measure motor shaft speed. This study proposes a new method for simplifying the instruments for motor bearing fault diagnosis. Specifically, a video clip recording of a running bearing system is captured using a cellphone that is equipped with a camera and a microphone. The recorded video is subsequently analyzed to obtain the instantaneous frequency of rotation (IFR). The instantaneous fault characteristic frequency (IFCF) of the defective bearing is obtained by analyzing the sound signal that is recorded by the microphone. The fault characteristic order is calculated by dividing IFCF by IFR to identify the fault type of the bearing. The effectiveness and robustness of the proposed method are verified by a series of experiments. This study provides a simple, flexible, and effective solution for motor bearing fault diagnosis. Given that the signals are gathered using an affordable and accessible cellphone, the proposed method is proven suitable for diagnosing the health conditions of bearing systems that are located in remote areas where specialized instruments are unavailable or limited.

1. Introduction

Bearings are vital components of rotating motors [1]. A survey shows that nearly 40% to 50% of motor failures are related to bearings [2]. Therefore, the conditions and faults of a motor bearing must be monitored and diagnosed to guarantee the safe operation and prevent further breakdowns of machines. In general, when a fault is located in a bearing, the collision among the bearing components, such as outer raceway, inner raceway, and rolling element, induces the impulses that can be detected in the acquired vibration or sound signal. When a defective bearing rotates at a constant speed, the generated impulses are periodic or quasi-periodic. The fault type of the bearing can be identified by examining the impulse repetition frequency or fault characteristic frequency (FCF) [3, 4]. In previous research, the energy operator demodulation approach, which is based on empirical mode decomposition, was used to decompose the defective signal, and then the FCF was identified in the envelope spectrum [5]. Stochastic resonance methods were also used to purify the noisy envelope signal and enhance the FCF for bearing fault diagnosis [3, 6–8]. The antisymmetric real Laplace wavelet method was introduced to attenuate the noise interference and reveal the FCF for the identification of different bearing faults [9]. A fast and adaptive varying-scale morphological analysis method was introduced for rolling element bearing fault diagnosis by enhancing the FCF [10].

However, when the frequency of rotation (FR) of the bearing changes with time, the impulses become nonperiodic and the instantaneous FCF (IFCF) changes with time accordingly. For instance, the rotating speeds of turbine rotors and shafts vary along with the shifts in the wind. Traditional frequency analysis methods, such as fast Fourier transform, are unsuitable for processing time-varying signals under

varying speeds. Several techniques have been proposed to address this issue, including order analysis (OA) methods, which have been widely deployed and proven effective for processing time-varying signals [11–13]. OA methods use the multiples of the rotating speed (orders) instead of the absolute frequencies as the frequency base. The spectral smearing that is induced by speed variation can be eliminated by resampling the signal at constant angular increments of a reference shaft. Before performing the OA methods, the precise instantaneous frequency of rotation (IFR) must be measured using a tachometer or an encoder. However, the installation and adjustment of these instruments can increase the measurement costs and may cause inconvenience. Therefore, several tacholess OA methods were used for extracting the IFR from the acquired vibration or sound signal. For instance, a previous work proposed a novel method that resampled the signal under a low speed fluctuation against the angle using the acceleration signal of a gearbox [14]. A tacholess order tracking method that was based on generalized demodulation was also introduced to extract the tachometer information from the vibration signal [15]. A rotating speed isolation method was proposed, in which the rotating speed component was separated using a low-pass filter and the IFR was extracted via ridge detection [16].

The above tacholess OA methods demonstrated a favorable performance in processing specific vibration signals, but these methods can only be applied if the fundamental frequency or harmonics of the bearing shaft are obviously shown in the vibration signals. Such a requirement may not always be satisfied in practice because the bearings that work in different lubrication conditions and mechanical loads may be subjected to various defects, and the vibration signals are usually contaminated by background noise. Therefore, the shaft speed information may be weak or even absent in the vibration signal. These insufficiencies limit the application of tacholess OA methods.

Given these drawbacks, this study proposes a new method that can perform fault diagnosis under varying speeds without using a tachometer or encountering the limitations of the traditional tacholess OA methods. This method only requires a cellphone that is equipped with a camera and a microphone. This method identifies the bearing fault as follows: (1) record a video of a running motor containing the bearing to be detected; (2) obtain the IFR from the video by calculating the correlation coefficients among the reference frame and the subsequent frames and then extracting the ridge from the time-frequency distribution (TFD) of the correlation coefficients; (3) obtain the IFCF from the audio track by filtering and demodulating the raw signal and then extracting the ridge from the TFD of the envelope signal; (4) finally, calculate the fault characteristic order (FCO) by dividing IFCF by IFR.

This study has two major contributions. First, it introduces the use of an accessible and affordable cellphone instead of specialized instruments (e.g., tachometer and accelerometer) for acquiring the IFR and IFCF synchronously. Second, this study proposes the FCO analysis method, which comprises advanced signal and image processing techniques, for diagnosing different bearing fault types under varying speeds. Several experiments are performed to verify the effectiveness, flexibility, and robustness of this method. As a standard electronic medium, videos can be easily recorded, compressed, copied, and broadcast. Therefore, the proposed method has potential applications in diagnosing the faults of bearing systems that are located in remote areas where specialized instruments are unavailable or limited.

The rest of the paper is organized as follows. Section 2 introduces the theoretical background and the algorithm flowchart of the proposed method. Section 3 verifies the effectiveness and robustness of the proposed method by performing a series of experiments, and then provides discussion. Section 4 draws the conclusions of the paper.

2. Proposed Method

First, a running motor containing the bearing to be detected is recorded on video using a cellphone as illustrated in Figure 1 (note that the coupling that connects the shafts of the motor and mechanical load must be uncovered). Second, the video and audio tracks are separated from the recording for further analysis.

2.1. Extract Rotating Speed Information from the Video Track. We can identify whether a motor is running or not by checking its rotating components, such as shaft, coupling, and shaft key. In accordance with this principle, the running rotating components that are recorded by the camera induce a pixel variation in different frames of the video track. We extract the FR from the video track by computing the correlation coefficients among the frames. The color RGB images are converted to grayscale images beforehand to reduce the computational cost [17]. Subsequently, an arbitrary frame is selected as the reference frame, which is denoted as follows:

$$F_r(x,y) = \begin{bmatrix} F_r(0,0) & \cdots & F_r(0,N-1) \\ \vdots & \cdots & \vdots \\ F_r(M-1,0) & \cdots & F_r(M-1,N-1) \end{bmatrix}, \quad (1)$$

where $M \times N$ is the resolution of the video. The sequential frames are denoted as $F_1(x,y), F_2(x,y), \ldots, F_k(x,y)$, respectively. The correlation coefficient r_i between $F_r(x,y)$ and $F_i(x,y)$ $(i = 1, 2, \ldots, k)$ is calculated as follows:

$$r_i = \frac{\sum_{x=0}^{M-1}\sum_{y=0}^{N-1}\left(F_r(x,y) - \overline{F}_r(x,y)\right)\left(F_i(x,y) - \overline{F}_i(x,y)\right)}{\sqrt{\left(\sum_{x=0}^{M-1}\sum_{y=0}^{N-1}\left(F_r(x,y) - \overline{F}_r(x,y)\right)^2\right)\left(\sum_{x=0}^{M-1}\sum_{y=0}^{N-1}\left(F_i(x,y) - \overline{F}_i(x,y)\right)^2\right)}}, \quad (2)$$

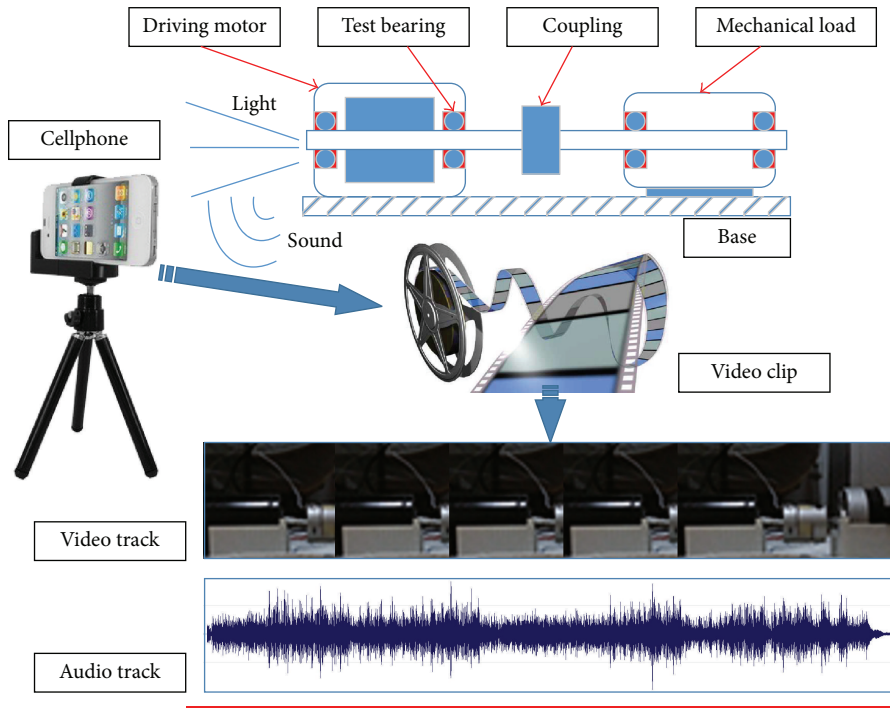

Figure 1: Framework of the proposed method.

where $\overline{F}_r(x, y)$ and $\overline{F}_i(x, y)$ are computed as follows:

$$\overline{F}_r(x, y) = \frac{\sum_{x=0}^{M-1} \sum_{y=0}^{N-1} F_r(x, y)}{M \times N},$$
$$\overline{F}_i(x, y) = \frac{\sum_{x=0}^{M-1} \sum_{y=0}^{N-1} F_i(x, y)}{M \times N}. \quad (3)$$

The calculated correlation coefficient reflects the pixel variation between $F_r(x, y)$ and $F_i(x, y)$. As the motor keeps running, the signal r_i will fluctuate in a specific range because the sequential frame, which is similar to reference frame, is recurring. Therefore, such a fluctuation can be used as a measurement of rotating speed.

2.2. Extract Envelope Signal from the Audio Track. The collision among the rotating components of the defective bearing generates impulse signals that excite the machine and induce resonance vibration synchronously. Therefore, the machine vibration frequency is modulated by the fault-induced impulse signal. The demodulated resonance technique is usually applied to identify the occurrence time of the impulses and obtain the FCF. From another aspect, the acquired bearing signal is always blurred by the background noise. Therefore, bandpass signal filtering is usually conducted before signal demodulation. Spectral kurtosis (SK) gives a measure of the impulsiveness of a bandpass filtered signal versus filter center frequency, with the values dependent on the filter bandwidth. The kurtogram gives the optimum combination of center frequency and bandwidth to maximize the SK. The range of combinations can be seen directly in the calculated kurtogram.

Here, the basis equation of SK is provided as

$$\mathrm{SK}_x = \frac{\left\langle |H(n, f)|^4 \right\rangle}{\left\langle |H(n, f)|^2 \right\rangle^2} - 2, \quad (4)$$

where $H(n, f)$ represents the complex envelope of a zero-mean nonstationary random process $s(n), n \in \mathbb{Z}$, at frequency f, the bracket $\langle \cdot \rangle$ denotes the temporal average of $s(n)$, and the constant -2 comes from the fact that $H(n, f)$ is a complex function. The fourth-order normalized cumulant in (4) indicates that the maximal SK is obtained when the strongest nonstationarities of the signal are revealed. Subsequently, the optimal filter with optimal central frequency (f_{opt}) and optimal bandwidth (Δf_{opt}) can be constructed by maximizing SK as follows:

$$\left(f_{\mathrm{opt}}, \Delta f_{\mathrm{opt}}\right) = \arg\max \left\{\mathrm{SK}\left(f, \Delta f\right)\right\}. \quad (5)$$

Several methods can be used in determining the optimal filter, such as the kurtogram based on short time Fourier transform [18], the fast kurtogram based on 1/3 binary filter banks [19], and the improved kurtogram based on wavelet packet transform (WPT) [20]. In this study the fast kurtogram method proposed by Antoni is used as it is a way of obtaining a limited set of combinations very efficiently [18, 19].

Applying SK-based signal filtering to the acquired sound signal attenuates the undesired noise outside of the resonance

band, thereby improving the signal-to-noise ratio (SNR) of the demodulated signal. This procedure is necessary because the defective bearing signal is recorded using a general-purpose microphone instead of a specialized directional one. Therefore, more background noise may be observed in the acquired signal, which consequently lowers the SNR of the signal. After signal filtering and signal demodulation, the envelope signal is finally obtained as $S_e(t)$.

2.3. IFR and IFCF Estimation from TFD and Ridge Extraction. Using the preceding methods, the rotating speed and envelope signal are extracted from the video and audio tracks, respectively. Given that the motor works under varying speeds, frequency domain analysis methods are unsuitable for processing these time-varying signals. Alternatively, TFD combines the information in both the time and frequency domains to analyze the nonstationary signal in bearing fault diagnosis [21]. Several techniques can be used to construct the TFD, such as short time Fourier transform (STFT), discrete wavelet transform (DWT), continuous wavelet transform (CWT) [22, 23], and WPT [24]. In this study, the STFT is utilized to construct the TFD of the envelope signal $S_e(t)$ as written in what follows:

$$\begin{aligned}\mathrm{STFT}\left\{S_e(t)\right\}(\tau,\Omega) &\equiv X(\tau,\Omega)\\ &= \int_{-\infty}^{\infty} S_e(t)\, w(t-\tau)\exp\left\{-j\Omega t\right\} dt,\end{aligned} \tag{6}$$

in which $w(t)$ is the window function. By choosing the proper window function, the two-dimensional TFD is constructed from the one-dimensional envelope signal.

Subsequently, a simple peak searching algorithm is employed to detect the ridge of the TFD image $L(i, j)$ using the following objective function [25]:

$$\underset{k\in[0,J-1]}{\mathrm{RE}}(k) = \arg\max_{h\in[h_0,I-1]}\left\{L(h,k)\right\}, \tag{7}$$

where the lower bound $h_0 \in \mathbb{Z}^+$ keeps the ridge search away from the distorted low frequency region in TFD. Given that the extracted ridge RE(k) may be subject to noise interference, a median filter is applied to RE(k) to smooth the curve as demonstrated in what follows:

$$\mathrm{RE}'(k) = \begin{cases}\mathrm{Median}\left[\mathrm{RE}\left(k-\dfrac{n-1}{2}\right),\mathrm{RE}\left(k-\dfrac{n-1}{2}+1\right),\ldots,\mathrm{RE}\left(k+\dfrac{n-1}{2}\right)\right], & n=1,3,5,7,\ldots\\ \mathrm{Median}\left[\mathrm{RE}\left(k-\dfrac{n}{2}\right),\mathrm{RE}\left(k-\dfrac{n}{2}+1\right),\ldots,\mathrm{RE}\left(k+\dfrac{n}{2}-1\right)\right], & n=2,4,6,8,\ldots,\end{cases} \tag{8}$$

where n is the order of the median filter.

The trend lines of IFR and IFCF can be obtained from the corresponding TFDs by performing ridge extraction. Moreover, considering that the frames per second (FPS) of the video are far less than the sampling frequency (f_s) of the audio, a downsampling strategy is applied to the IFCF trend line to reduce its sampling frequency from f_s to FPS. Using this strategy, the data lengths of the IFR and IFCF trend lines are equal, which facilitates the FCO calculation. The FCO is then calculated as follows:

$$\mathrm{FCO} = \frac{\mathrm{IFCF}}{\mathrm{IRF}}. \tag{9}$$

Given that the FCO only relies on the physical structure of the bearing, the FCO is a constant for a specific bearing. The FCOs for the bearing with inner and outer raceway faults are, respectively, calculated as follows:

$$\mathrm{FCO_I} = \frac{n_r}{2}\left(1+\frac{D_1}{D_2}\cos\alpha\right), \tag{10}$$

$$\mathrm{FCO_O} = \frac{n_r}{2}\left(1-\frac{D_1}{D_2}\cos\alpha\right), \tag{11}$$

where n_r is the number of rollers, D_1 and D_2 are the diameters of one rolling element and the pitch diameter of the bearing, respectively, and α is the bearing contact angle.

2.4. Method Summary. The proposed method is illustrated in Figure 2. By conducting a series of signal processing and image processing algorithms, the trend lines of the IFR and IFCF are extracted, while the FCO, which reflects the bearing fault type, is obtained. Several experiments are performed to verify the effectiveness and robustness of the proposed method in application.

3. Experimental Verification and Discussion

3.1. Experimental Setup. The experimental setup is shown in Figure 3. The cellphone used in this setup was an iPhone 5s (Apple Inc.) that can capture videos of 1280 × 720 pixels (720 p) at 120 FPS and with an audio sampling frequency of 44.1 kHz. A brushless DC motor (BLDC) drives a healthy DC generator (mechanical load), and the torque is transferred through coupling. The cellphone was placed parallel to the test rig, and the distance between the cellphone and the coupling is denoted by d as shown in Figure 3. A lux level meter was used to measure environment illumination. The test bearing was mounted in the drive-end of the BLDC. The motor is driven by a controller-fed BLDC driver. Motor speed is controlled by adjusting the output voltage that is generated by a digital-to-analog converter (DAC) that is embedded in the controller (STM32F407VGT6, STMicroelectronics Inc.). The specifications of the BLDC and test bearing are listed in Tables 1 and 2, respectively. Artificial faults (width: 0.6 mm) were set using wire electrode discharge machining in the outer and inner raceways of two separate bearings. Bearings with an inner race fault, an outer race fault, and a healthy bearing were tested in the experiment. After substituting the

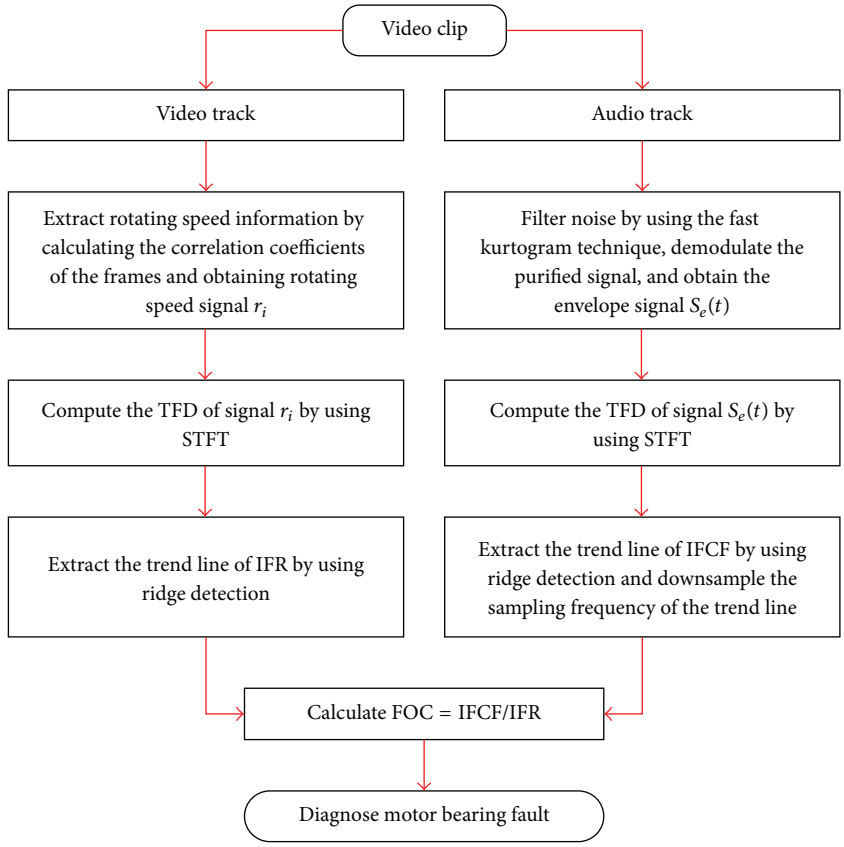

Figure 2: Algorithm flowchart of the proposed method.

bearing parameters into (10) and (11), FCO_I and FCO_O are calculated as 4.43 and 2.57, respectively.

3.2. Case Study: Defective Bearing Tests. Two defective bearings with outer and inner raceway faults were tested to verify the effectiveness of the proposed method. Distance d was set as 0.3 m, while the environment illumination was measured as ~417 lux in this study and the following case studies (~417 lux means that the illumination may slightly deviate in each experiment). For the bearing with an outer raceway fault, the correlation coefficients r_i that were calculated from the video frames are shown in Figure 4. The values of r_i are close to 1, which indicates small deviations among the frames [most regions in the images are still, except for the rotating (moving) shaft and coupling]. Given that the features of the shaft and coupling recur in the video frames as the motor keeps running, r_i fluctuates within a specific range. This fluctuation reflects the motor operation and can be used as a measurement of rotating speed. The TFD of r_i is plotted in Figure 5 by employing STFT algorithm, in which the IFR curve can be clearly observed. The trend line of IFR was obtained by performing ridge extraction, as shown in Figure 6. The trend line signifies that the motor works in varying speeds.

Subsequently, the sound signal from the separated audio track was analyzed to identify the FCF. The raw signal and its kurtogram are shown in Figures 7 and 8, respectively. The kurtogram constructs the optimal filter through which the noise is attenuated and the transient signatures are retained. The envelope signal that was generated from the optimal filtered signal is displayed in Figure 9, while its TFD is shown in Figure 10. The IFCF and its harmonics are revealed in the TFD, but the noise interference can be noticed. After extracting the ridge and then applying the median filter to the ridge signal, the trend line of the IFCF was obtained as shown in Figure 11. The FCO was calculated from the corresponding points of the extracted trend lines of IFR and IFCF using (11). The mean value of the calculated FCOs is 2.60, which is close to the theoretical FCO of outer raceway faults (2.57). In other words, a fault occurs in the outer raceway, thereby confirming the effectiveness of the proposed method.

The bearing signal with an inner raceway fault was analyzed to confirm the flexibility of the proposed method. The motor speed in Figure 12 was configured differently from that in Figure 4. The IFR can be clearly recognized in the TFD as shown in Figure 13, and the trend line of the IFR was extracted as shown in Figure 14. The sound signal was subsequently filtered using the optimal filter that was constructed from the kurtogram. The demodulated signal is displayed in Figure 15. The TFD of the envelope signal [Figure 16] presents the IFCF and its harmonics. The trend line of IFCF is eventually extracted as shown in Figure 17. By dividing the IFCF by IFR, the averaged FCO is calculated as 4.40, which is close to the theoretical value (4.43). Therefore, the

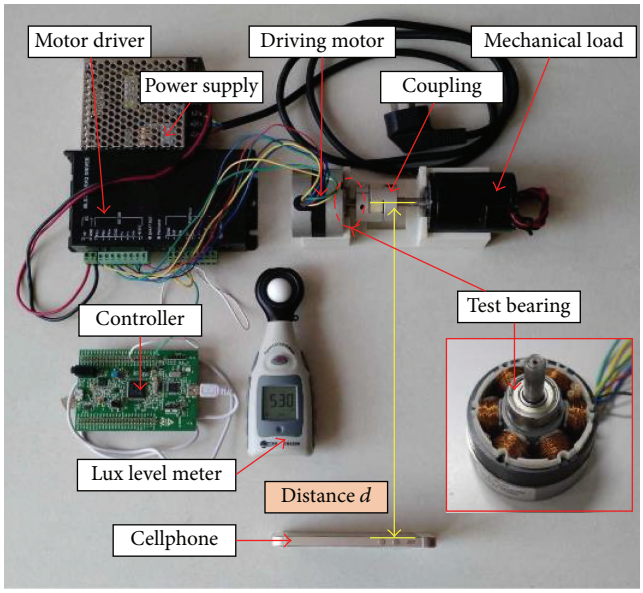

Figure 3: Experimental setup.

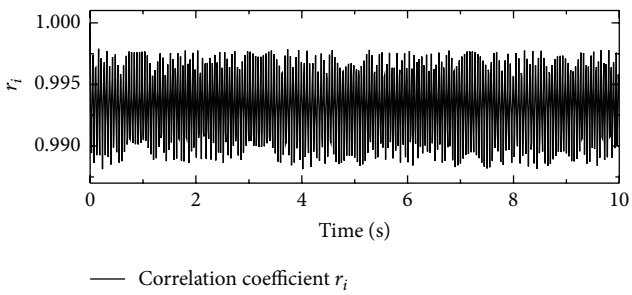

Figure 4: Correlation coefficients r_i of the outer raceway fault bearing.

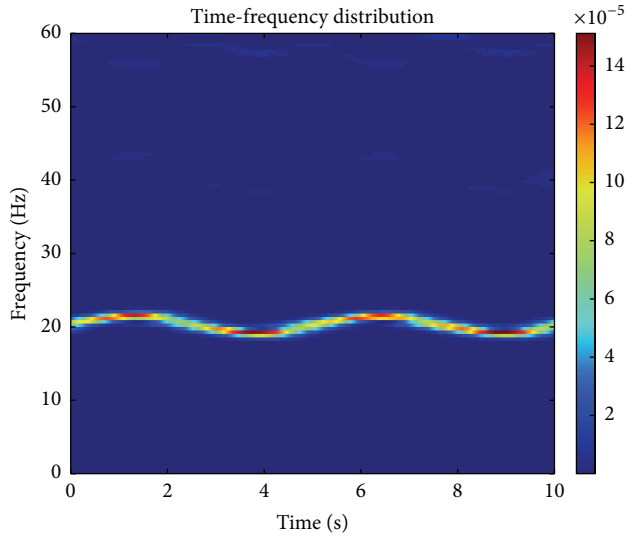

Figure 5: TFD of r_i of the outer raceway fault bearing.

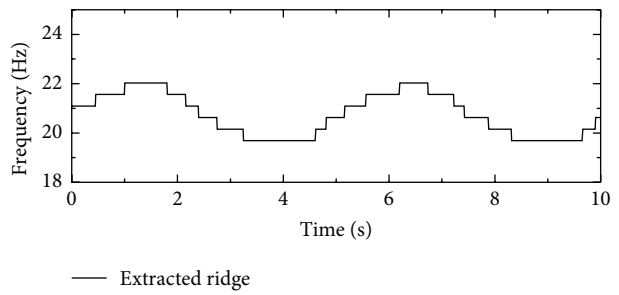

Figure 6: Trend line of the IFR of the outer raceway fault bearing.

Table 1: Parameters of BLDC.

Type	Number of poles	Number of phases	Rated voltage	Rated torque
57BL01	4	3	24 VDC	0.057 Nm

bearing is subjected to an inner raceway fault, which reconfirms the effectiveness of the proposed method.

3.3. Case Study: Healthy Bearing Test. The two cases above indicate that the proposed method can detect the motor bearing fault under varying speeds. However, in practice, most operating bearings are healthy. Therefore, the bearing fault diagnosis method must not trigger any false alarms when the bearing operates favorably. A healthy bearing is tested in this subsection to verify the robustness of the proposed method. Following the same analysis procedure, the results of the healthy bearing test are presented in Figures 18–23. Figures 18–20 show that IFR is clearly in TFD and that the trend line is extracted precisely by conducting ridge extraction, which indicates that the extraction of IFR from the video frames that are recorded by the camera demonstrates a stable performance. The envelope signal in Figure 21 has a smaller amplitude than the defective signals, which signifies that the impulse components that are generated by the collisions in the defective bearing have high energies that induce the high amplitude of the recorded signal. The TFD of the envelope signal is shown in Figure 22. By performing ridge extraction and filtering the extracted curve using the median filter, the trend line is obtained and presented in Figure 23. After dividing the trend line in Figure 23 by that in Figure 20, the averaged order is calculated as 3.94, which indicates that the trend line of Figure 23 is fourth-order harmonic of the IFR. This harmonic is induced from the BLDC motor with four poles. From another aspect, despite the roughness of the trend line from the sound signal, a relatively accurate order can still be calculated by averaging the abundant corresponding points in the trend lines.

The results of the preceding case studies are synthetically provided in Figure 24. The theoretical orders are plotted in lines, whereas the measured orders are represented by various shapes. The measured order curve of the outer raceway fault signal has a favorable consistency with the theoretical line. The measured order curves of the inner raceway fault and healthy signals fluctuate in specific ranges that are centered at the corresponding theoretical lines. Fault detection (whether a fault exists or not) and fault isolation (type of fault in the

Table 2: Parameters of the test bearing.

Type	Outside diameter	Inside diameter	Roller diameter	Number of rollers	Contact angle
608Z	22 mm	8 mm	3.97 mm	7	0

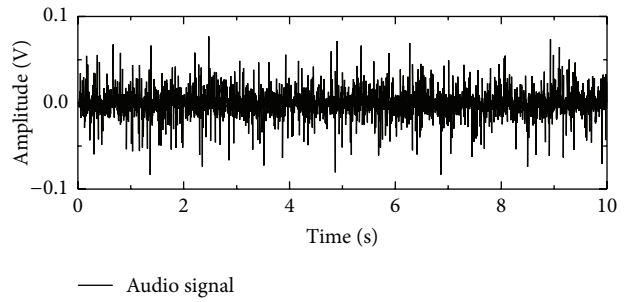

Figure 7: Audio signal of the outer raceway fault bearing.

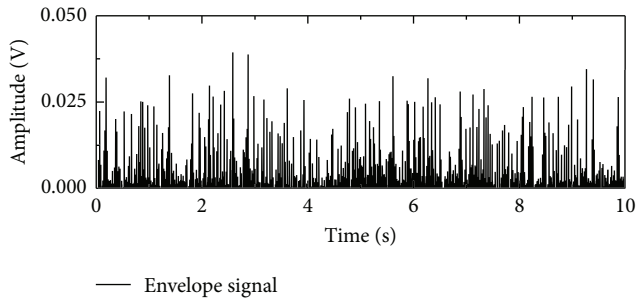

Figure 9: Envelope signal of the outer raceway fault bearing.

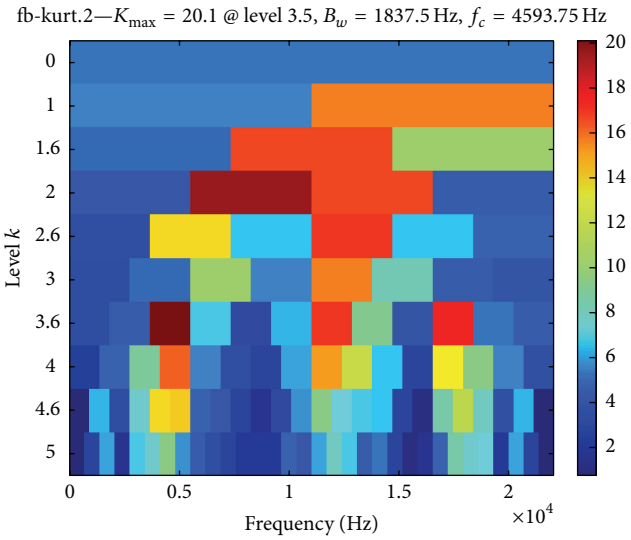

Figure 8: Kurtogram of the audio signal of the outer raceway fault bearing.

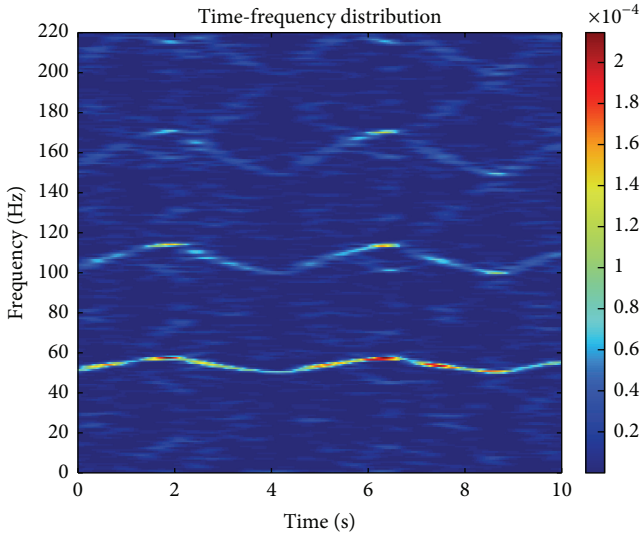

Figure 10: TFD of the envelope signal of the outer raceway fault bearing.

bearing) can be achieved by calculating the mean values of the measured curves. Therefore, the effectiveness and robustness of the proposed method have been verified by the experiments.

3.4. Quantitative Analysis. In this study, a commercial cellphone is used to record a video for diagnosing a bearing fault. The experimental results indicate that fault detection and isolation can be accomplished by analyzing the video and audio tracks that are separated from the video clip. However, the camera and microphone that are used in this study are designed for general purposes. Therefore, their properties must be examined further to guarantee that the proposed method can be effectively implemented in practice. Apparently, distance d between the cellphone and the tested bearing affects the qualities of both the video and audio, whereas the environmental illumination affects the video quality. The effects of these two factors are investigated in this subsection.

3.4.1. Distance Test. In this test, distance d varied from 0.2 m to 0.8 m with an increase step of 0.1 m, whereas the environment illumination remained constant at ~457 lux. Bearings with different conditions, including outer raceway fault, inner raceway fault, and healthy bearings, were tested separately. To quantitatively analyze a test set, a criterion, success rate (Sr), is introduced and defined as follows:

$$\mathrm{Sr} = \frac{T_s}{T_t} \times 100\%, \tag{12}$$

where T_s and T_t represent the times of successful tests and the times of total tests in a test set, respectively. The test is considered successful if the measured FCO or rotating speed order ranges between 97% and 103% of the corresponding theoretical order. Each test set contains 10 tests in which the

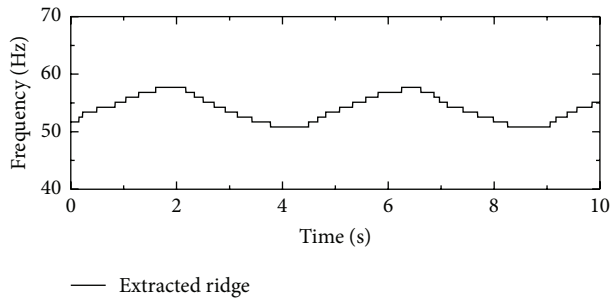

Figure 11: Trend line of the IFCF of the outer raceway fault bearing.

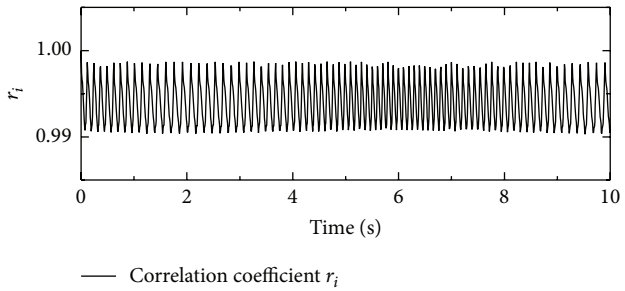

Figure 12: Correlation coefficients r_i of the inner raceway fault bearing.

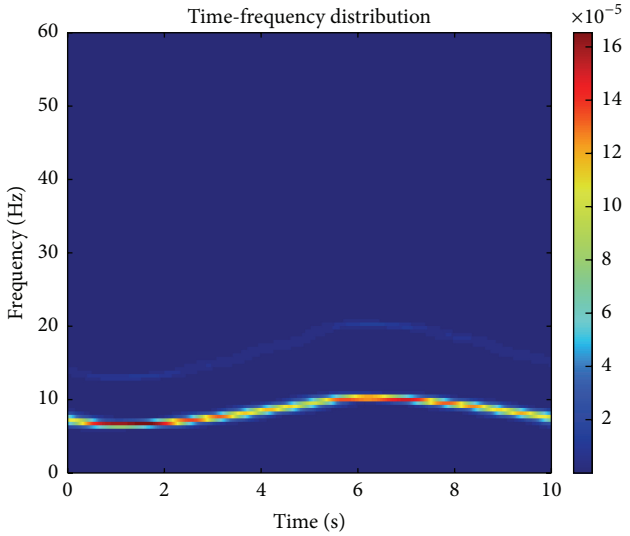

Figure 13: TFD of r_i of the inner raceway fault bearing.

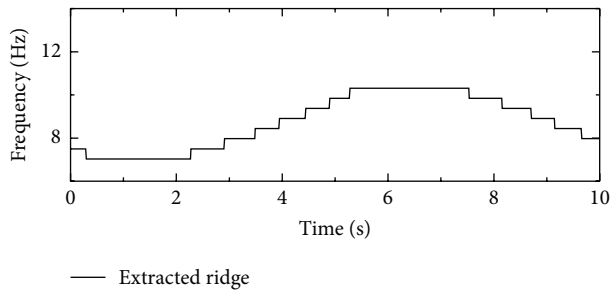

Figure 14: Trend line of the IFR of the inner raceway fault bearing.

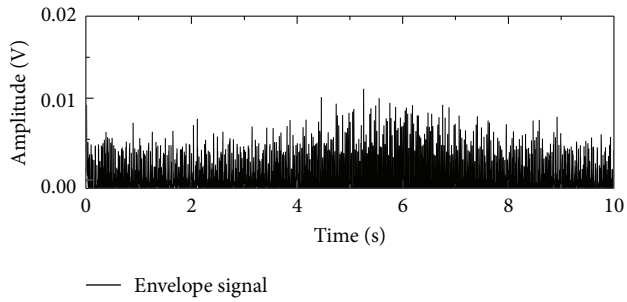

Figure 15: Envelope signal of the inner raceway fault bearing.

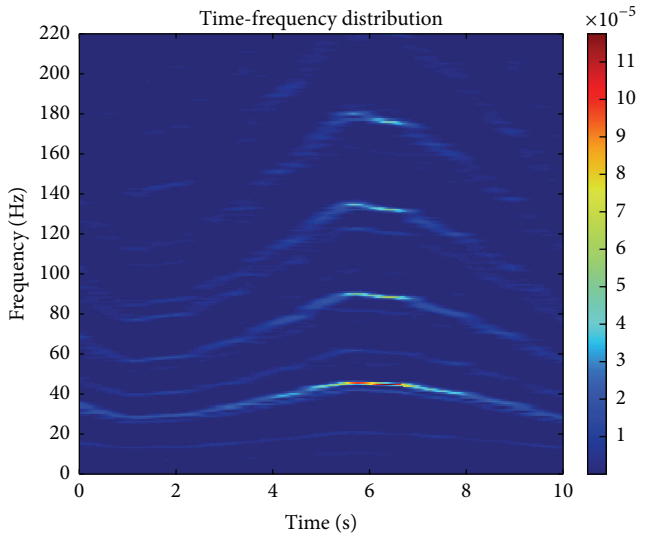

Figure 16: TFD of the envelope signal of the inner raceway fault bearing.

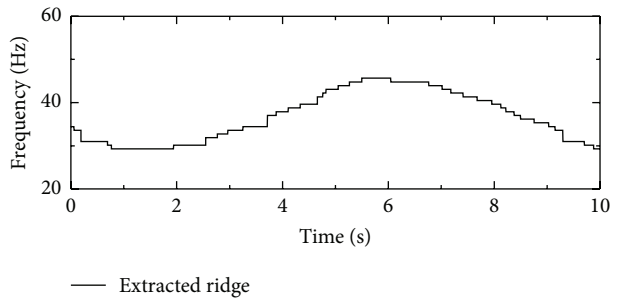

Figure 17: Trend line of the IFCF of the inner raceway fault bearing.

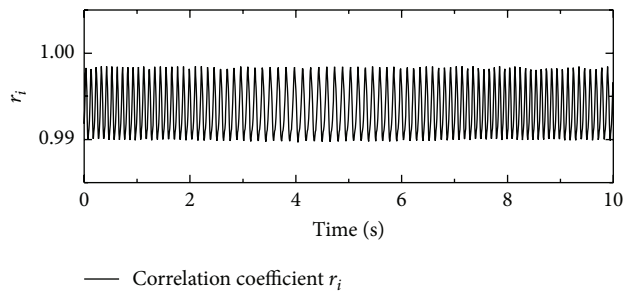

Figure 18: Correlation coefficients r_i of the healthy bearing.

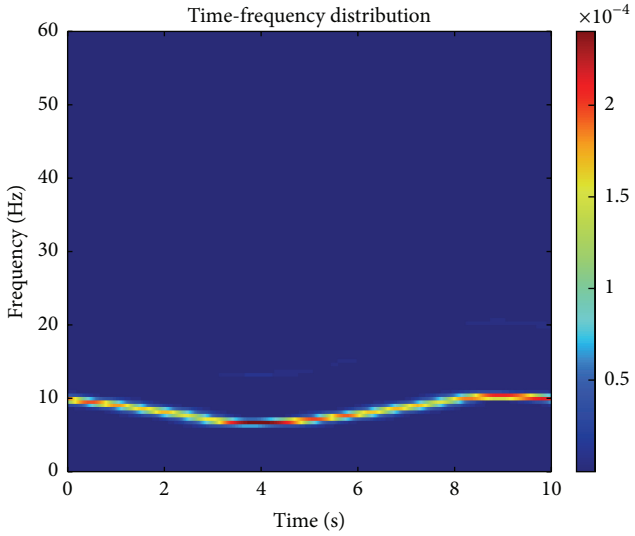

Figure 19: TFD of r_i of the healthy bearing.

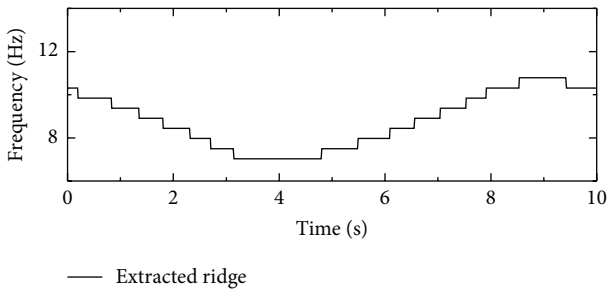

Figure 20: Trend line of the IFR of the healthy bearing.

Table 3: Success rate at different distances.

d (m)	0.2	0.3	0.4	0.5	0.6	0.7	0.8
Outer raceway	100%	100%	100%	100%	100%	100%	100%
Inner raceway	100%	100%	100%	100%	100%	70%	0%
Healthy bearing	100%	100%	80%	0%	0%	0%	0%

motor ran in different speed modes (e.g., speed up, speed down, and their combinations) and various durations. The results are summarized in Table 3. The detection of the outer raceway fault demonstrates the highest flexibility for different distances. By contrast, the proposed method fails to recognize the healthy bearing when $d \geq 0.4$ m because the sound attenuates along with increasing distance. Therefore, the healthy bearing signal has a lower amplitude than the defective bearing signals, thereby preventing the microphone from effectively recording the sound signal that is generated from the bearing. The results indicate that placing the cellphone as close as possible to the test bearing can improve the fault detection success rate.

3.4.2. Environment Illumination Test. The previous test shows that distance d significantly affects the quality of the sound signal that is recorded by the microphone. Given that we use the cellphone camera to record the running motor,

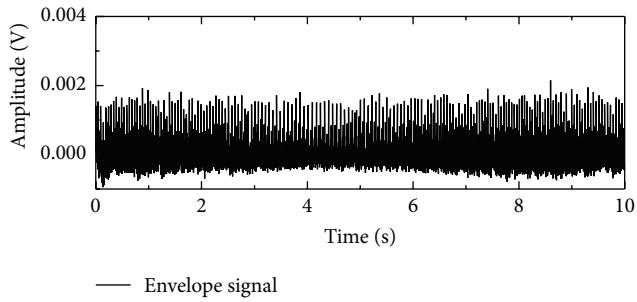

Figure 21: Envelope signal of the healthy bearing.

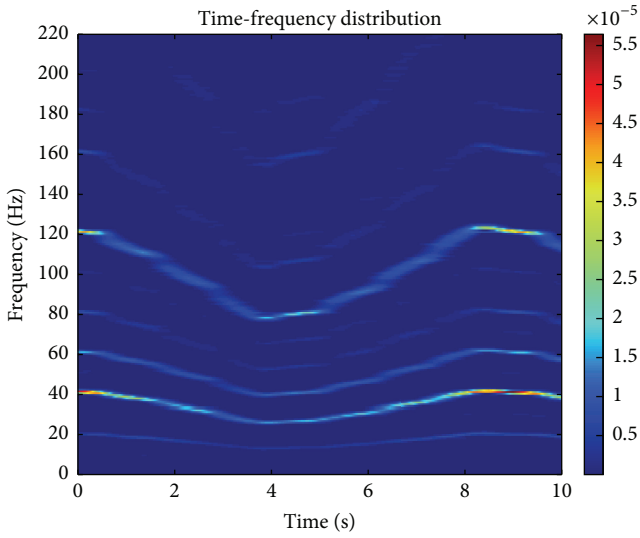

Figure 22: TFD of the envelope signal of the healthy bearing.

environment illumination is a critical factor that affects the video quality. Therefore, illumination experiments were conducted to evaluate the effectiveness of the proposed method. We moved the test rig to different indoor areas to achieve different illuminations. The camera flash was turned off at all times, and distance d remained constant at 0.3 m. Similar to the preceding test, each test set contains 10 tests, and the experimental results are presented in Table 4. The success rates for all illuminations are 100%. The color RGB image is converted to grayscale one before processing, and the correlation coefficient is only determined by the relative differences among the frames. Therefore, the illumination variation within a specific range does not affect the diagnosis of bearing fault. Following the joint International Organization for Standardization/International Commission on Illumination (ISO/CIE) standard for the lighting of indoor work places [26], we take the "Power Stations" in which motors or generators are widely used as examples. Given that the recommended luminance for "Power Stations" ranges from 50 lux to 500 lux, the proposed method shows potential to be used in practical applications.

3.5. Discussion. Several deficiencies and possible solutions must also be noted when adopting the proposed method.

Table 4: Success rate at different illuminations.

Illumination (lux)	~97	~318	~579	~968
Outer raceway	100%	100%	100%	100%
Inner raceway	100%	100%	100%	100%
Healthy bearing	100%	100%	100%	100%

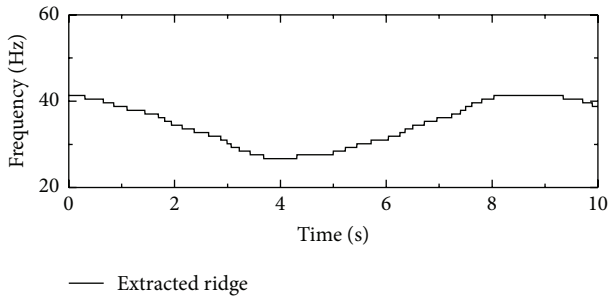

Figure 23: Trend line of the IFCF of the healthy bearing.

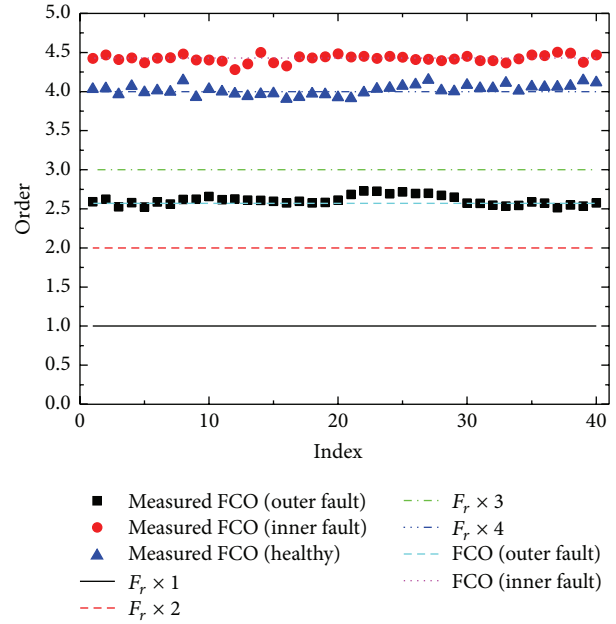

Figure 24: Order analysis of the healthy and the defective bearing signals.

First, according to the Nyquist sampling theorem, the maximal supported motor speed is 3000 rpm when the sampling frequency of the camera is 120 FPS. To diagnose a bearing in a motor that runs faster than 3000 rpm, a camera with a higher FPS must be used, such as the 240 FPS iPhone 6 camera (Apple Inc.). Second, the cellphone microphone is omnidirectional, which may induce obvious background noise interference. The microphone must be placed as close as possible to the test bearing. Third, the rotating component, for example, the coupling used in this study, is used as the indicator to measure the rotating speed of the motor. In this circumstance, the harmonics of the FR may be stronger than the fundamental FR due to possible symmetry of the coupling. This could be avoided by attaching a paper label on the coupling or the shaft. Finally, additional investigations on both hardware and software should be conducted to enhance the effectiveness of the proposed method in practical applications. For instance, the computational capability of a cellphone is comparable to that of a personal desktop computer; thus, the algorithms that are used in this study can be transferred to the cellphone to accomplish a real-time mobile computation, which will provide convenience for visual fault diagnosis on a cellphone APP. This work should be conducted in future research.

4. Conclusion

A simplified method for diagnosing motor bearing faults is proposed in this study. The proposed method diagnoses the bearing fault as follows: (1) a running motor containing the test bearing is recorded on video; (2) the IFR is obtained from the video by calculating the correlation coefficients and extracting the ridge from the TFD of the correlation coefficients; (3) the IFCF is obtained from the audio track by filtering and demodulating the raw signal and then extracting the ridge from the TFD of the envelope signal; (4) finally, FCO is calculated by dividing IFCF by IFR. Both qualitative analysis and quantitative analysis have been conducted to verify the effectiveness and robustness of the proposed method. The experimental data are gathered from an accessible and affordable cellphone to enable the fault diagnosis for bearing systems that are located in the remote areas where specialized instruments are unavailable or limited.

Competing Interests

The authors declare that there are no competing interests regarding the publication of this paper.

Acknowledgments

This work was supported in part by the Natural Science Foundation of Anhui Province (nos. 1608085QE110 and 1508085SQE212), in part by the Startup Funding for Talents of Anhui University, in part by the National Natural Science Foundation of China (no. 51505001), and in part by the Program for New Century Excellent Talents in University (NCET-13-0539).

References

[1] S. Zhang and W. Li, "Bearing condition recognition and degradation assessment under varying running conditions using NPE and SOM," *Mathematical Problems in Engineering*, vol. 2014, Article ID 781583, 10 pages, 2014.

[2] S. Nandi, H. A. Toliyat, and X. D. Li, "Condition monitoring and fault diagnosis of electrical motors—a review," *IEEE Transactions on Energy Conversion*, vol. 20, no. 4, pp. 719–729, 2005.

[3] S. Lu, Q. He, and F. Kong, "Stochastic resonance with Woods–Saxon potential for rolling element bearing fault diagnosis," *Mechanical Systems and Signal Processing*, vol. 45, no. 2, pp. 488–503, 2014.

[4] S. B. Wang, G. G. Cai, Z. K. Zhu, W. G. Huang, and X. W. Zhang, "Transient signal analysis based on Levenberg-Marquardt method for fault feature extraction of rotating machines," *Mechanical Systems and Signal Processing*, vol. 54-55, pp. 16–40, 2015.

[5] C. Junsheng, Y. Dejie, and Y. Yu, "The application of energy operator demodulation approach based on EMD in machinery fault diagnosis," *Mechanical Systems and Signal Processing*, vol. 21, no. 2, pp. 668–677, 2007.

[6] S. Lu, Q. He, H. Zhang, and F. Kong, "Enhanced rotating machine fault diagnosis based on time-delayed feedback stochastic resonance," *Journal of Vibration and Acoustics*, vol. 137, no. 5, Article ID 051008, 2015.

[7] H. Zhang, Q. He, S. Lu, and F. Kong, "Stochastic resonance with a joint Woods-Saxon and Gaussian potential for bearing fault diagnosis," *Mathematical Problems in Engineering*, vol. 2014, Article ID 315901, 17 pages, 2014.

[8] S. Lu, Q. He, F. Hu, and F. Kong, "Sequential multiscale noise tuning stochastic resonance for train bearing fault diagnosis in an embedded system," *IEEE Transactions on Instrumentation and Measurement*, vol. 63, no. 1, pp. 106–116, 2014.

[9] D. Wang and Q. Miao, "Smoothness index-guided Bayesian inference for determining joint posterior probability distributions of anti-symmetric real Laplace wavelet parameters for identification of different bearing faults," *Journal of Sound and Vibration*, vol. 345, pp. 250–266, 2015.

[10] C. Shen, Q. He, F. Kong, and W. T. Peter, "A fast and adaptive varying-scale morphological analysis method for rolling element bearing fault diagnosis," *Journal of Mechanical Engineering Science*, vol. 227, no. 6, pp. 1362–1370, 2013.

[11] K. R. Fyfe and E. D. S. Munck, "Analysis of computed order tracking," *Mechanical Systems and Signal Processing*, vol. 11, no. 2, pp. 187–202, 1997.

[12] J. J. Wang, R. X. Gao, and R. Q. Yan, "Multi-scale enveloping order spectrogram for rotating machine health diagnosis," *Mechanical Systems and Signal Processing*, vol. 46, no. 1, pp. 28–44, 2014.

[13] T. Wang, M. Liang, J. Li, and W. Cheng, "Rolling element bearing fault diagnosis via fault characteristic order (FCO) analysis," *Mechanical Systems and Signal Processing*, vol. 45, no. 1, pp. 139–153, 2014.

[14] F. Bonnardot, M. El Badaoui, R. B. Randall, J. Danière, and F. Guillet, "Use of the acceleration signal of a gearbox in order to perform angular resampling (with limited speed fluctuation)," *Mechanical Systems and Signal Processing*, vol. 19, no. 4, pp. 766–785, 2005.

[15] M. Zhao, J. Lin, X. Q. Xu, and Y. Lei, "Tacholess envelope order analysis and its application to fault detection of rolling element bearings with varying speeds," *Sensors*, vol. 13, no. 8, pp. 10856–10875, 2013.

[16] Y. Wang, G. Xu, Q. Zhang, D. Liu, and K. Jiang, "Rotating speed isolation and its application to rolling element bearing fault diagnosis under large speed variation conditions," *Journal of Sound and Vibration*, vol. 348, pp. 381–396, 2015.

[17] R. C. Gonzalez, *Digital Image Processing*, Pearson Education India, 2009.

[18] J. Antoni and R. B. Randall, "The spectral kurtosis: application to the vibratory surveillance and diagnostics of rotating machines," *Mechanical Systems and Signal Processing*, vol. 20, no. 2, pp. 308–331, 2006.

[19] J. Antoni, "Fast computation of the kurtogram for the detection of transient faults," *Mechanical Systems and Signal Processing*, vol. 21, no. 1, pp. 108–124, 2007.

[20] Y. G. Lei, J. Lin, Z. J. He, and Y. Y. Zi, "Application of an improved kurtogram method for fault diagnosis of rolling element bearings," *Mechanical Systems and Signal Processing*, vol. 25, no. 5, pp. 1738–1749, 2011.

[21] Q. He, Y. Liu, Q. Long, and J. Wang, "Time-frequency manifold as a signature for machine health diagnosis," *IEEE Transactions on Instrumentation and Measurement*, vol. 61, no. 5, pp. 1218–1230, 2012.

[22] J.-D. Wu and J.-C. Chen, "Continuous wavelet transform technique for fault signal diagnosis of internal combustion engines," *NDT & E International*, vol. 39, no. 4, pp. 304–311, 2006.

[23] J. Lin and L. Qu, "Feature extraction based on morlet wavelet and its application for mechanical fault diagnosis," *Journal of Sound and Vibration*, vol. 234, no. 1, pp. 135–148, 2000.

[24] R. Yan, R. X. Gao, and X. Chen, "Wavelets for fault diagnosis of rotary machines: a review with applications," *Signal Processing*, vol. 96, pp. 1–15, 2014.

[25] A. Zhang, F. Hu, Q. B. He, C. Q. Shen, F. Liu, and F. R. Kong, "Doppler shift removal based on instantaneous frequency estimation for wayside fault diagnosis of train bearings," *Journal of Vibration and Acoustics*, vol. 136, no. 2, Article ID 021019, 2014.

[26] International Organization for Standardization, "Lighting of indoor work places," ISO 8995:2002(E)/CIE S 008/E-2001, International Organization for Standardization, 2002.